LBNL-41439
Preprint

ERNEST ORLANDO LAWRENCE
BERKELEY NATIONAL LABORATORY

UV Photodissociation Dynamics of Allyl Radical by Photofragment Translational Spectroscopy

Domenico Stranges, Martin Stemmler, Xueming Yang, James D. Chesko, Arthur G. Suits, and Yuan T. Lee

Chemical Sciences Division

February 1998

Submitted to
Journal of Chemical Physics

DISCLAIMER

LBNL-41439

UV Photodissociation Dynamics of Allyl Radical by Photofragment Translational Spectroscopy

Domenico Stranges,[a] Martin Stemmler, Xueming Yang,[b]
James D. Chesko, Arthur G. Suits, and Yuan T. Lee

Chemical Sciences Division
Ernest Orlando Lawrence Berkeley National Laboratory
University of California
Berkeley, California 94720

February 1998

Present addresses:
[a]Dipartimento di Chimica, Università "La Sapienza," and Centro Studi Termodinamica Chimica alle Alte Temperature - CNR, Dipartimento di Chimica, Università "La Sapienza," P.le A. Moro 5, Rome I-00185, Italy.
[b]Institute of Atomic and Molecular Sciences, Academia Sinica, P.O. Box 23-166, Taipei, Taiwan, ROC.

This work was supported by the Director, Office of Energy Research, Office of Basic Energy Sciences, Chemical Sciences Division, of the U.S. Department of Energy under Contract No. DE-AC03-76SF00098.

ABSTRACT

Photodissociation of the allyl radical, CH_2CHCH_2, has been studied using the method of molecular beam photofragment translational spectroscopy following excitation to the C(2 $^2B_1$) and A(1 $^2B_1$) states by 248 and 351 nm photons. Two different primary channels have been detected at 248 nm excitation: H-atom loss (84%) and CH_3 elimination (16%). From the product translational energy distribution and polarization dependence studies dissociation processes from the ground state C_3H_5 potential energy surface are inferred for both wavelengths. At 248 nm there may also be a contribution to the H-atom loss channel from predissociation by a higher electronic excited state. RRKM calculations show that the formation of cyclopropene is not important while formation of allene and methylacetylene from 1- and 2-propenyl radicals dissociation are important reaction pathways at both wavelengths. Evidence for CH_3 elimination directly from an allylic structure through a four-member cyclic transition state is present in the translational energy distribution peaked well away from zero.

I. INTRODUCTION

It is well known that neutral free radicals are important intermediate species in many important chemical processes. However very often, only limited information is available on these "transient" species (as compared to stable molecules) mainly due to the difficulties to produce them in well defined conditions suitable for definitive experimental studies.

The allyl radical is the simplest conjugated π-electron hydrocarbon radical and represents a benchmark molecule for both theoretical and experimental studies. It is an intermediate in many thermal[1], combustion[2], photochemical[3] and surface catalitic[4,5] reactions. The allyl radical has been the subject of many experimental and theoretical investigations. Electron-spin resonance (ESR)[6,7] and electron diffraction[8] showed that this radical has a planar structure with C_{2v} symmetry in its ground state. Photoelectron spectroscopy[9] has been used to determine the vertical and adiabatic ionization potentials. Vibrational frequencies and structural information for the ground electronic state have

been obtained from matrix infrared (IR),[10,11] ultraviolet (UV) resonant Raman spectroscopy,[12-16] and IR diode laser spectroscopy.[17] Currie and Ramsay[18] measured the absorption spectrum of the allyl radical in the 410-370 nm region. A system of diffuse bands in that region were assigned to the A ($1\ ^2B_1$) ← X ($^2A_2$) electronic transition. Other vibronic bands have also been detected in the 210-250 nm region.[19] Oscillator strengths of several UV bands have been measured experimentally.[20,21] The resonant multiphoton ionization (MPI) technique was used to probe the one photon forbidden transition B ($3s\ ^2A_1$) ← X ($^2A_2$)[22,23] with a (2+2) scheme. Three fundamental vibrational levels in both the ground and excited states were identified. Recently Chen and coworkers reported an extensive high resolution spectroscopic study on this radical.[24-26] They have produced a supersonic molecular beam of allyl radical by flash pyrolysis[27] of allyl iodide. From their partially rotationally resolved MPI spectra they were able to assign many vibronic bands in the 250-240 nm region and to deduce the band origins of the strongly interacting B ($3s\ ^2A_1$), C ($2\ ^2B_1$), and D($1\ ^2B_2$) electronic states.

Several theoretical studies at different levels of calculations have analyzed the ground state structure and vibrational frequencies.[28-34] The a*b initio* MO-CI[35] and spin-coupled valence-bond (SCVB)[36] methods have also been used to study the ground and excited electronic states of the allyl radical. The energies of the excited electronic states were obtained, which are in good agreement with the experimental results.[18,25]

Another interesting aspect of the allyl radical is the possible isomerization into cyclopropyl radical through an electrocyclic reaction.[37-39] From the Woodward-Hoffmann rules,[40] based on MO symmetry considerations, both conrotatory and disrotatory pathways are symmetry forbidden on the ground state potential energy surface so that the ground state of each radical correlates with an electronic excited state of the other.[41] However, the thermal ring opening of cyclopropyl radical into allyl radical has been observed experimentally and the activation energy was estimated to be about 20 kcal/mol.[42] This result also agrees with an *ab initio* calculation[39] in which an highly nonsymmetric transition state was found.

Very recently Deyerl et al.[43] have investigated the photodissociation of the allyl radical at 248.15 nm. The H-atom loss channel have been detected with an average translational energy release of 13.9 kcal/mol. Despite all the experimental and theoretical

studies described above, a full picture on the primary photochemical processes of the allyl radical is still lacking.

In the present work we report a study on the photodissociation of the allyl radical at 248 and 351 nm excitation by photofragment translational spectroscopy (PTS).

II. EXPERIMENT

The experimental measurements in this work were carried out on a rotating source photofragment-translational spectrometer which has been described previously in detail.[44,45] A simple schematic drawing of the experimental setup is shown in Fig. 1. Briefly, a pulsed molecular beam of the allyl radical (C_3H_5) seeded in helium was skimmed twice before entering the main chamber where it was crossed at 90° with a focused pulsed laser beam. Neutral photofragments scattered from the laser-molecular beam interaction region and which fly along the detector axis are ionized by an electron bombardment ionizer at a distance of 36.7 cm from the interaction region. The ions produced in the ionizer are then mass selected by a quadrupole mass spectrometer, and counted with a Daly ion detector. A 486 personal computer interfaced multichannel scaler (Turbo-MCS, EG&G Ortec) triggered by the laser pulse is used to collect and store the time-of-flight (TOF) spectra. Product laboratory angular distributions can be obtained by rotating the molecular beam source around the laser propagation axis, which is perpendicular to the plane defined by the molecular beam direction and the detector axis. The allyl radical pulsed beam was generated from the pyrolysis of allyl iodide (C_3H_5I). The pyrolytic source used in this experiment (Fig. 2) is an adaptation to our pulsed valve[46] of the one designed by Chen *et al.*[27] A mixture of C_3H_5I/He ~ 0.2% was expanded at a stagnation pressure of 760 torr through a resistively heated SiC tube helded at 1400-1500 K, as determined by beam TOF. Under these conditions C_3H_5I pyrolyses quantitatively to produce an allyl radical and iodine atom. The mass spectra of the molecular beam with the nozzle unheated (upper trace) and heated (lower trace) are shown in Fig. 3. The quantitative loss of C_3H_5I (m/e = 168) and the appearance of I^{++} peak (m/e=63.5) in the heated mass spectrum are a strong evidence for the formation of the allyl radical, since doubly charged ions are much more likely to come from one atom

than from the dissociative ionization of C_3H_5I. The molecular beam velocity and its velocity spread were measured by the time-of-flight technique with a spinning slotted disk. Different parts of the gas pulse can be sampled by changing the delay between the wheel and the pulsed valve so that optimum experimental conditions are achieved. The delay between the pulsed valve and the laser trigger can be calculated from the wheel angular velocity and the delay between the pulsed valve and the wheel. The beam velocity was measured to be ~ 3300 m/s with a full width half-maximum (FWHM) velocity spread of 17%.

In all the experiments performed in this work the molecular beam was crossed at 90° by an output of a Lambda Physik EMG 103 MSC excimer laser operating at the KrF (248 nm) and XeF (351 nm) transitions. A convex lens (25 cm focal length) was used to focus the laser beam to a 2.5×6 mm spot in the interaction region, with fluence of 50-100 mJ/cm^2/pulse for studies at 248 nm excitation and 100-200 mJ/cm^2/pulse for studies at 351 nm excitation. The output of the excimer laser was polarized using a pile of ten quartz plates at Brewster's angle with respect to the direction of laser propagation, yielding >95% polarized light. The polarization direction of the laser beam can be rotated with respect to the detector axis by adjusting the orientation of the polarizer.

Time-dependent background, arising from the dissociative ionization of pulsed C_3H_5 from the molecular beam, was present in TOF spectra at masses ≤ 41 (C_3H_5) and at small angles. The shot-by-shot background subtraction method was used, which has been described in detail elsewere[47]. Briefly, the pulsed valve was run twice as fast as the laser in repetition rate. A TOF spectrum with laser-on and laser-off was recorded, and the laser-off TOF was then subtracted from the laser-on TOF.

A forward convolution technique was used to fit the data. Briefly, a trial center-of-mass translational energy distribution is convoluted with the instrumental response functions and molecular beam conditions to yield a calculated TOF spectrum in the laboratory reference frame, which is then compared to the experimental spectrum. The translational energy distribution is iteratively adjusted until a good fit is obtained.

At 248 nm excitation, the intensity of all detected fragments from C_3H_5 photodissociation varied linearly at lower laser power, but showing saturation effect at higher laser power. At 351 nm excitation the intensity of C_3H_4 detected fragments (see

below) varied linearly with the laser power up to the maximum power of the excimer laser showing that the absorption cross section at this wavelength should be quite small. The TOF spectra reported in this work have been recorded under conditions where saturation effects were absent.

H and D atoms produced in photodissociation experiments are difficult to detect by mass spectrometry for two main reasons. The signal is very low (kinematics factor) and the inherent background inside the detector at those masses is very high. The only way to increase the signal-to-noise ratio (S/N) is to increase the number density of the parent molecules by reducing the distance between the nozzle and the interaction region. H-atom TOF spectra have been measured with success in our group on several systems[48] but always on crossed molecular beam type machines[49] because of the space available in the fixed source chamber. We have slightly modified our experimental apparatus (also called "Rotating Source Machine") in order to detect H-atom time-of-flight, the C_3H_4 momentum-matched photofragment. The modification is done by simply adding an extension to the source chamber (Fig. 4). In the modified setup, the pulsed valve is located upward inside this box. Two small holes exist along the laser beam propagation direction to let the laser beam pass through and a third hole is present along the detector axis to let photofragments going to the detector. In this configuration the molecular beam, the laser beam, and the detector axis are all perpendicular to each other. The 1.5 mm diameter laser spot is located at a distance of 1 cm from the nozzle. While the H-atom detection was not successful for the allyl radical, due to a low number density of the parent molecule, H-atom TOF spectra from the photodissociation of other systems were recorded.[50] Moreover, the same configuration was used to detect H and D atoms from the photolysis of HI and DI at 248 nm in order to determine experimentally the instrumental response functions (the ionizer width and the neutral flight distance) of our apparatus. In Fig. 5 the H- and D-atom TOF spectra from photodissociation of HI and DI at 248 nm excitation are shown. From the peak positions of the two spin-orbit components, the neutral flight distance (the bond dissociation energy, D_O, of the two channels are well known[51]) is determined to be 36.7 cm, and from the widths of the two peaks the ionizer width can also be determined to be 0.9 cm.

III. RESULTS AND ANALYSIS

In all the TOF spectra presented here, the open circles represent the experimental data, the dashed lines are single channel contributions to the forward convolution fit, and the solid lines are the overall fit to the data.

248 nm Excitation

At 248 nm excitation two primary dissociation channels are present (see below). For the H-atom loss channel, TOF spectra were collected for products at m/e = 41-38 ($C_3H_5^+$, $C_3H_4^+$, $C_3H_3^+$, $C_3H_2^+$) at detector angles, Θ, of 2.5°, 3°, 4°, 5°, 6°, and 7.5° from the molecular beam. TOF spectra at m/e = 41 were recorded in order to check if the signal observed at lower masses came from the photodissociation of the allyl radical or from heavier hydrocarbon molecules. The low signal at this mass (~2% of m/e = 40)) is due only to ^{13}C natural abundance in C_3H_4 neutral fragments. TOF spectra at m/e = 40-38 show a single peak and they are identical when recorded at the same laboratory angle, suggesting that they all originate from the same neutral fragment by electron impact dissociative ionization inside the ionizer. TOF spectra at m/e = 39 and 38 have the best S/N. Fig. 6 shows the TOF spectra for m/e 38 at Θ = 3°, 5°, 6°, and 7.5°. The number of laser shots necessary for each spectrum ranged from 25,000 (at small Θ) to 100,000 (at larger Θ). The center-of-mass (c.m.) translational energy distribution, $P(E_T)$, used to fit these TOF spectra is shown in Fig. 7. It is peaked around 0 kcal/mol and has a tail that decreases monotonically up to 59 kcal/mol. The 0-2.5 kcal/mol range of the $P(E_T)$ is not reported because C_3H_4 fragments with translational energy, E_T, lower than 2.5 kcal/mol are not scattered outside 2.5° from the molecular beam. The mean translational energy release, $\langle E_T \rangle$, for this channel is 13.2 kcal/mol and represents an upper limit for the reasons mentioned before.

For the $CH_3 + C_2H_2$ channel both momentum-matched photofragments have been detected. TOF spectra for m/e 26 (Θ = 7.5°, 15°, 20°, 25°, and 30°) and 15 (Θ = 30°) have been collected after 300,000 (m/e 26) and 1,500,000 (m/e 15) laser shots. In Fig. 8, the TOF spectra collected for m/e 26 at 7.5°, 15°, 20° and 30° are presented. At Θ = 7.5°

two different peaks, centered around 80 and 120 μs, are clearly resolved. At larger Θ only one single peak is present. The Newton diagram is shown in Fig. 9, with circles representing the highest possible velocities of the photofragments when all the available energy is channeled into translation. For the H-atom loss channel the C_3H_4 product can be allene and/or methylacetylene (see Section IV). It is clear from the coparison with TOF of C_3H_4 that the slow component in the TOF at m/e = 26 and 7.5° is due to C_3H_4 dissociative ionization and its contribution can be fitted with the $P(E_T)$ shown in Fig. 7. The $P(E_T)$ used to fit the acetylene channel is shown in Fig. 10. It has a totally different shape as compared to the H-atom loss channel. It is peaked at 16 kcal/mol, $\langle E_T \rangle \sim 19.1$ kcal/mol, with a FWHM of 20.5 kcal/mol, and extends up to 62.0 kcal/mol. The same $P(E_T)$ has also been used to fit the TOF spectrum at m/e = 15 (Fig. 11), showing that it is the the momentum-matched counterpart of acetylene.

In order to determine the branching ratio, R, between the two primary dissociation channels the TOF spectrum at m/e = 26 and 7.5° was used because both contributions were recorded under the same experimental conditions. R was calculated according to Eq. (1)[52] where σ_a^O and σ_b^O are the relative cross sections of fragments a and b monitored at a given m/e ratio and corrected for kinematics.

$$R = (\sigma_a/\sigma_b) = (\sigma_a^O/\sigma_b^O)(Q_b/Q_a)(F_b/F_a) \qquad (1)$$

Q_a and Q_b are the ionization cross sections of the products which result in fragment a and b and were calculated using the method of Fitch and Sauter.[53] F_a and F_b are the probabilities of products to fragment in the ionization process to form fragments *a* and *b* at the given m/e ratio. We estimate the uncertainty in the branching ratio obtained in this way to be ± 25%. The ratio σ_a^O/σ_b^O (calculated by our analysis program) depends on the anisotropy parameter β, even if unpolarized light is used.[54] Polarization dependence studies were done for m/e = 38, Θ=4°, and m/e = 26, Θ=20°. The polarization direction of the light can be rotated in the plane defined by the molecular beam and the detector axis. The anisotropy parameter is obtained directly from the laboratory angular

distribution[55] $I(\gamma)$:

$$I(\gamma) \propto 1 + \beta P_2(\cos(\gamma - \gamma_o))$$

where γ is laboratory polarization angle, γ_o is the correction angle for the c.m. to laboratory transformation, and $P_2(\gamma - \gamma_o)$ is the second Legendre polynomial in $\cos(\gamma - \gamma_o)$. For the acetylene plus methyl (CH_3) channel we did not observe any dependence of the angular distribution from the polarization angle, indicating that this dissociation process is isotropic ($\beta = 0$). For the H-atom loss channel, a very small negative anisotropy parameter β, -0.05, has been observed.

The branching ratio between the H-atom loss channel and the acetylene plus methyl channel at 248 nm excitation is determined to be 0.84 : 0.16.

351 nm Excitation

At the 351 nm excitation only H-atom loss channel was observed. TOF spectra were recorded for m/e = 40-38 at detector angles of 2.5°, 3°, 4°, 5°, and 6° from the molecular beam. Modulated background was also subtracted shot-by-shot. At 351 nm the available energy for the same asymptotic products is 33.5 kcal/mol lower as compared to 248 nm. The Newton circle will be smaller and the neutral C_3H_4 photofragments can be scattered only up to 6° from the molecular beam. TOF spectra obtained here show only a single peak, and they are identical for different m/e values when collected at the same laboratory angle. In Fig. 12, TOF spectra at m/e=39 and Θ = 2.5, 3°, 4°, and 6° are shown. The number of laser shots necessary for each spectrum ranges from 200,000 to 400,000. The c.m. translational energy distribution used to fit these TOF spectra is shown in Fig. 13. It has a similar shape as compared to the H-atom loss $P(E_T)$ at 248 nm. It peaks near 0 kcal/mol and decreases monotonically up to 24.5 kcal/mol. The upper limit for the mean translational energy release at 351 nm excitation is determined to be $\langle E_T \rangle$ = 4.5 kcal/mol. The anisotropy parameter measured for this channel was zero.

RRKM Calculations

In order to establish the relative importance of possible isomerization and dissociation reaction channels from the ground state potential energy surface (PES) of the C_3H_5 system (see section IV) we have performed RRKM calculation to determine the microcanonical rate constants k(E)'s for all the reaction pathways shown in Fig. 14. The lack of *ab initio* calculations at the same level of theory for all reaction pathways on the ground state C_3H_5 PES required us to choose empirical methods to estimate vibrational frequencies and structures for the different radical species and transition states (TS's). The vibrational frequencies for the allyl radical have been taken from Ref. 10, 11, 13, and 34. For the cyclopropyl radical from Ref. 56. Vibrational frequencies for the 1- and 2-propenyl radicals were obtained from propylene removing one C-H stretch and two C-H bending vibrational modes. For k_1, k_5, k_6, k_7, k_8, and k_{10} the TS's have been defined following the prescriptions given by Pearson and Rabinovitch.[57] TS's for the isomerization reactions among the allyl radical and the 1- and 2-propenyl radicals (through 1,3 and 1,2 H-atom migration, respectively) have been built in a similar way as Ibuki *et al.*[58] The TS for allyl-cyclopropyl isomerization (k_9, k_{-9}) was taken halfway. For the dissociation of allyl radical into C_2H_2 + CH_3 (k_2) through a four-member cyclic TS we have adopted a similar procedure used for k_3 and k_4 TS's with an additional lowering of CH_2 wagging, twisting and rocking vibrations. In Tab. 1, the calculated rate constants for 248 and 351 nm together with energetic information and A-factors are reported. Some of the isomerization and dissociation reactions have been investigated previously[59] with RRKM theory, and our results are in agreement with these results. In order to get branching fractions for the formation of allene, methylacetylene, cyclopropene, and acetylene, a set of differential equations for the reaction rates has been solved with the Laplace transform method,[60] and the results are listed in Tab. 2. For the 248 nm case the initial condition in which only the allyl radical is present is reported here (assuming cyclopropil radical as the initial molecular species present, the branching fraction values change less than one percentage units, so that the global picture does not change).

IV. DISCUSSION

As mentioned above Chen's group[24-26] reported a detailed spectroscopic study of the allyl radical in the 240-250 nm region by resonant MPI. The band origin for the C (2 $^2B_1$) state was found to be 248.15 nm. The broadband KrF excimer laser used here certainly covers this transition. Several weaker and broader vibronic bands has also been observed at shorter wavelengths. The absorption cross section increases at shorter wavelengths, reaching a maximum at ~222 nm.[21] The results by a gas-phase resonant Raman study at 225 nm are consistent with isomerization to cyclopropyl radicals.[12] The longer lifetime of the C state at longer wavelengths could be due to the presence of a barrier for the electrocyclization transformation by a disrotatory mode.[41] In this case the C state decay could be through Internal Conversion (IC) to form vibrationally hot allyl radicals either in the ground state or in the A state.[43]

Allyl radical in the ground electronic state with 115.3 kcal/mol of vibrational energy can either dissociate or isomerize. A schematic energetic diagram with possible dissociation and isomerization processes is showm in Fig. 15. Thermochemical data have been taken from Ref.'s 59 and 61, and corrected to 0 K (see also Tab. 1). There are two possible dissociation channels directly from an allylic structure: H-atom loss to form allene, reaction (1), and CH_3 elimination through a concerted mechanism, reaction (2). The allyl radical can isomerize by an electrocyclic transformation through an highly nonsymmetric TS[39] into cyclopropyl radical, reaction (9), or into 1- and 2-propenyl radicals through an H-atom shift, reaction (4) and (3) respectively. Finally, cyclopropyl radical can loose an H-atom to form cyclopropene, reaction (10); 1-propenyl radical ($\bullet CHCHCH_3$) can either loose the H-atom attached to the central carbon atom to form metylacetylene, reaction (8), or can brake the C-C bond to form C_2H_2 and CH_3, reaction (6); 2-propenyl radical ($CH_2C\bullet CH_3$) can loose an H-atom to form either methylacetylene, reaction (7), or allene, reaction (5). There are five different reaction pathways that produce an H-atom and allene/methylacetylene/cyclopropene, and two for the formation of acetylene plus the methyl radical.

$$CH_2CHCH_2(X\,^2A_2) \rightarrow CH_2CCH_2\,(X\,^1A_1) + H(^2S) \qquad (1)$$

$CH_2CHCH_2(X\,^2A_2) \rightarrow C_2H_2\,(X\,^1\Sigma_g^+) + CH_3(X\,^2A_2")$ (2)

$CH_2CHCH_2(X\,^2A_2) \rightarrow CH_2C\bullet CH_3(X)$ (3)

$CH_2CHCH_2(X\,^2A_2) \rightarrow \bullet CHCHCH_3(X)$ (4)

$CH_2C\bullet CH_3 \rightarrow CH_2CCH_2\,(X\,^1A_1) + H(^2S)$ (5)

$\bullet CHCHCH_3 \rightarrow C_2H_2\,(X\,^1\Sigma_g^+) + CH_3(X\,^2A_2")$ (6)

$CH_2C\bullet CH_3 \rightarrow CHCCH_3(X\,^1A_1) + H(^2S)$ (7)

$\bullet CHCHCH_3 \rightarrow CHCCH_3(X\,^1A_1) + H(^2S)$ (8)

$CH_2CHCH_2(X\,^2A_2) \rightarrow$ c-C3H5($X\,^2A'$) (9)

c-C3H5($X\,^2A'$) $\rightarrow$ c-C_3H_4(X) + $H(^2S)$ (10)

The $P(E_T)$ for the H-atom loss channel (Fig. 7) is peaked around zero and extended up to the thermodynamic limit for allene/methylacetylene + H formation. This observation suggests that both molecular species may be formed as the final products. From the maximum E_T value it is not possible to establish if the less endothermic dissociation channel, CH_3CCH + H, is present. This is due to the small difference (1.5 kcal/mol) between the enthalpy of formation (ΔH_0) of allene and that of methylacetylene. Cyclopropene is less stable than allene/metylacetylene of about 21-22 kcal/mol, therefore the available energy for reaction (10) should be reduced by the same amount. This means that if this channel is present it should contribute at lower E_T. We do not observe any change of the slop of the $P(E_T)$ around the thermodynamic limit for this channel (E_T~37 kcal/mol), moreover the branching fraction obtained from RRKM calculations (Tab. 2) is < 1%. This low value is mainly due to the lower rate constant k_{10} for dissociation as compared to the isomerization reaction k_{-9} (Tab. 1). The same RRKM calculations show that allene and methylacetylene are produced in almost equal amounts through an extensive isomerization before dissociation. More than 50% of the dissociation events do not came from allyl radicals directly. While the shape of the $P(E_T)$ is in qualitative agreement with a statistical dissociation, the mean translational energy release of 13.2 kcal/mol, in good agreement with what has been observed previously,[43] and a slightly negative anisotropy parameter are in apparent contradiction to the statistical dissociation picture. An RRKM type $P(E_T)$, which was calculated assuming no barrier on the exit

channel, predicts an $<E_T>$ of ~5 kcal/mol.[62] Even if we assume that all the potential energy barrier for the reverse reaction is channeled into translation, the predicted $<E_T>$ will be only ~7-8 kcal/mol, that is still less than the experimental value. The transition moment of the C ($2\ ^2B_1$) ← X ($^2A_2$) transition is perpendicular to the C_{2v} axis and in the molecular plane[35] (M_y-type transition). Prompt dissociation to form allene plus an H-atom from the ground state geometry would yield β=-1. As we all know, the anisotropy parameter β will go to zero for a dissociation process with its dissociation time longer than the rotational period of the parent molecule. This kind of behavior is expected for dissociation processes from the ground electronic states after an internal conversion decay mechanism from an electronic excited state. The higher $<E_T>$ value found experimentally and a β slightly negative may be due to a competition between two different micro-dissociation mechanisms: internal conversion and predissociation through an excited electronic state. In this case, the anisotropy distribution measured should come from two different contributions, one isotropic ($\beta = 0$) and another with $\beta < 0$. For the allyl radical the only rotation that can change the angle between the initial direction of the transition moment and the final direction of the C-H bond, prior to break apart, is around the axis perpendicular to the molecular plane. The classical rotational period around this axis, assuming a rotational temperature of 150 K, is 4.2 ps. From the partially rotationally resolved spectra we have estimated a lifetime for the C state at 248 nm of 1-2 ps. This shows that predissociation should be faster than the rotational period showing up in a substantial negative value of β for the dissociation process.

Internal conversion of the C state to the first low lying electronic excited A($1\ ^2B_1$) state will produce allyl radicals with 11.4 kcal/mol of vibrational energy. Currie and Ramsay[18] observed a number of diffuse vibronic bands in the 410-370 nm region, which were assigned to the A($1\ ^2B_1$) ← X($^2A_2$) transition. The resolution of their spectrophotometer is high enough to resolve rotational structures[18] and they concluded that predissociation, to form allene plus an H-atom, could be responsible of the diffuseness of those bands. Irradiation of allyl radicals trapped in an Ar-matrix with 410 nm light was shown to produce new vibrational bands in the IR spectrum assigned to cyclopropyl radical.[56] Orbital correlation diagram for the interconversion of allyl and

cyclopropyl radicals[40,41] shows that the A state of the allyl radical correlates with the ground state of the cyclopropyl radical along the conrotatory mode, suggesting that the ring closure process will be fast (symmetry allowed). This conclusion is also supported by *ab initio* calculations at the CASSCF level.[63] The main result of this calculation shows that the conrotatory pathway has no barrier along the reaction coordinate, and the disrotatory pathway has a barrier less than 1.5 kcal/mol. Their conclusion was that the cyclization process would be feasible and also responsible to the diffuse character of the vibronic bands of the first absorption transition instead of predissociation. As mentioned above by changing the initial conditions for the solution of the set of differential equations, with the cyclopropyl radical as the only molecular species initially present instead of the allyl radical, the global picture will not change. The only small difference is that the branching fraction for reaction (10) rises to 1%.

The second primary dissociation channel detected at 248 nm excitation is the formation of acetylene and the methyl radical. This accounts for 16% of the total dissociation events. In the studies on the thermal decomposition of the allyl radical,[59] the formation of acetylene has been observed. It was supposed to come only from 1-propenyl radical dissociation, reaction (6). The $P(E_T)$ for this channel obtained in this work is peaked at 16 kcal/mol (Fig. 10). The barrier for the CH_3 addition reaction to C_2H_2 to form 1-propenyl radical has been found to be 7.7 kcal/mol.[64] This also represents the barrier on the exit channel for the reverse reaction. The upper limit for the most probable E_T for the dissociation of 1-propenyl into acetylene and CH_3 can be estimated to be about 7.7 kcal/mol assuming that all the potential energy barrier is channeled into translation. This value is certainly much less than what have been observed in this work. Our $P(E_T)$ suggests the existence of a tighter TS for this dissociation channel. A possible candidate for this transition state is a four-member cyclic TS where one CH_2 group is rotated of about 90°. Dissociation of the allyl radical can occur through reaction (2) where C_2H_2 and CH_3 are produced directly from the allyl radical through this four-member cyclic TS. The proposed TS structure is similar to the one for H_2 elimination reaction from ethylene where the $P(E_T)$ was found to be peaked at 20 kcal/mol.[65] The $P(E_T)$ peak position represents a lower limit to the potential energy barrier height. The asymmetry of the TS for reaction (2) will couple efficiently the reaction coordinate with the other internal

degrees of freedom suggesting that the true barrier will be consistently higher and the products should be rotationally and vibrationally excited. The total branching fraction for this channel obtained from RRKM calculations (Tab. 2) is 26.4%, higher than the value determined experimentally. Moreover, 9.6% of the 26.4% fraction is due to reaction (6) according to the RRKM calculations. Even though the TOF spectra at m/e = 26 (Fig. 8) and the $P(E_T)$ do not show any bimodality, a contribution from reaction (6) can still be present especially at low E_T. We have simulated TOF spectra with two different contributions, one with a $P(E_T)$ peaked at 16 kcal/mol for reaction (2) and the other peaked at ~5 kcal/mol for reaction (6). Although this simulation procedure has certain degree of arbitrariness, it shows that the contribution of reaction (6) will be likely less than 15-20% of the total for this channel, which is still somewhat lower than the calculated value. The calculated contribution of reaction (6) can be lowered by increasing the barrier for the isomerization between the allyl and 1-propenyl radicals and/or choosing a tighter TS for reaction (6). The branching fractions reported in Tab. 2 have been calculated by considering only statistical dissociation reactions from the ground potential energy surface, therefore they do not include a possible contribution to the H-atom loss channel from predissociation. The higher branching fraction for the acetylene channel, as compared to the experimental value, may be due to that the barrier assumed for reaction (2) is too low for the RRKM calculations (20 kcal/mol). The dissociation products will be internally extremely hot, since on average about 77% of the available energy for the H-atom loss channel will be deposited to internal excitation (mainly vibrational excitation), and about 72% of the available energy for the acetylene plus CH_3.

The absorption of a 351 nm photon excites the allyl radical to the $A(1\ ^2B_1)$ state. The A state decays through an electrocyclic transformation to the ground state of cyclopropyl radical with 53.4 kcal/mol of vibrational energy. The lack of angular distribution dependence on the laser polarization angle γ ($\beta = 0$), a $P(E_T)$ peaked around zero, and a mean translational energy of 4.5 kcal/mol are all consistent with this mechanism for the H-atom loss channel. In fact, a sub picosecond predissociation process to form allene plus an H-atom will show up with a negative β (the A state has the same symmetry of the C state). An RRKM type $P(E_T)$ for reactions (1), (8), (7), and (5), which

are assumed barrierless, predict a $<E_T>$ = 2.5 kcal/mol. If we add ~2 kcal/mol for the repulsive interaction due to the small exit barrier, the agreement with the experimental value is very good. The threshold for the formation of cyclopropene plus an H-atom, reaction (10), is 49.9 kcal/mol. Assuming a barrier of 3 kcal/mol for the reverse reaction, the available energy to overcome this barrier is only 0.5 kcal/mol. The rate constant for reaction (10), k_{10}, will be so low (Tab. 1) that cyclopropene formation will not compete with the isomerization into ground state allyl radical through a nonsymmetric TS, k_{-9}. RRKM calculations show that isomerization of the allyl radical with 81.5 kcal/mol vibrational energy is extensive. Only 18% of the dissociation products (Tab. 2) came from an allylic structure. Methylacetylene is predicted to be the most abundant product with 41.6% yield, allene 27.3%, and acetylene 31.1% (with 29.9% from dissociation of the 1-propenyl radical). The inability to detect signal at m/e = 26 may be due to different reasons. If the barrier to the isomerization between the allyl and the 1-propenyl radicals is higher, the branching fraction for the acetylene channel will then be reduced. From a comparison of the signal levels for m/e = 38-39 at 248 and 351 nm, we can conclude that the absorption cross section of the allyl radical at 351 nm will be ~100 times smaller than 248 nm, which is in agreement with previous results.[35] The kinematics also play an important role. For the H-atom loss channel the signal of the heavy fragment is concentrated in only 6 degrees in the laboratory reference frame, while the Newton circle for C_2H_2 extends up to 40 degrees.

At the 351 nm excitation the dissociation products will still be internally hot, since on average ~82% of the available energy will be channeled into C_3H_4 internal excitation (mainly vibrational excitation).

V. CONCLUSION

Photodissociation of the allyl radical has been studied by photofragment translational spectroscopy following excitation to the C(2 $^2B_1$) and A(1 $^2B_1$) states. At 248 nm excitation two different primary channels have been detected: H-atom loss (84%) and CH_3 elimination (16%). The overall shape of the $P(E_T)$ for the H-atom loss channel suggests a statistical dissociation from the ground potential energy surface of the C_3H_5

system. The decay mechanism of the excited state is either through internal conversion into the ground state or internal conversion into the A state followed by an electrocyclic transformation into ground state cyclopropyl radical and, finally, reopening of the ring to form the allyl radical in the ground state with 115.3 kcal/mol of vibrational energy. The small negative anisotropy parameter β and the higher mean translational energy release $\langle E_T \rangle$, as compared to an RRKM type calculated value, can be rationalized by the competition between two different decay mechanisms for the C state: internal conversion and predissociation through a higher excited state. RRKM calculations show that almost 50% of allyl radicals dissociate to give allene plus an H-atom and acetylene plus CH_3, while the remaining radicals isomerize into 1- and 2-propenyl radicals before dissociation to form allene and methylacetylene plus an H-atom. The $P(E_T)$ for the acetylene plus CH_3 channel is peaked away from zero at 16 kcal/mol and is due mainly to dissociation from an allylic structure. This result, supported also by RRKM calculations, has been interpreted by a dissociation process from an allylic structure through a cyclic four-member transition state. A smaller contribution to this channel could also come from dissociation of the 1-propenyl radical.

The A state of allyl radical is reached after excitation at 351 nm. The decay mechanism is again an electrocyclic transformation into ground state cyclopropyl radical, followed by a reopening of the ring to form the allyl radical in the ground state with 81.5 kcal/mol vibrational energy. RRKM calculations also show that isomerization into the 1- and 2-propenyl radical is extensive with final production of methylacetylene and allene plus an H-atom.

ACKNOWLEDGMENTS

D. S. gratefully acknowledges the *Consiglio Nazionale delle Ricerche* (Italy) for a fellowship. This work was supported by the Director, Office of Energy Research, Office of Basic Energy Science, Chemical Science Division of the U. S. Department of Energy under Contract No. DE-AC03-76SF00098.

REFERENCES

[1] W. Tsang, Int. J. Chem. Kint. **10**, 1119 (1978).

[2] M. Weissman and S. W. Beson, Prog. Energy Combust. Sci. **15**, 273 (1989).

[3] R.E. Linder, D.L. Winters, and A.C. Ling, Can. J. Chem. **54**, 1405 (1976).

[4] R.N. Carter, A.B. Anton, and G. Apai, J. Am. Chem. Soc. **114**, 4410 (1992).

[5] J.C. Schultz and J.L. Beauchamp, J. Chem. Phys. **87**, 3587 (1983).

[6] R. W. Fessenden and R. H. Schuler, J. Chem. Phys. **39**, 2147 (1963).

[7] M. J. McManus, R. W. Fessenden, and D. M. Chipman, J. Phys. Chem. **92**, 3778 (1988).

[8] E. Vajda, j. Tremmel, B.Rozsondai, I. Hargittai, A. K. Maltsev, N. D. Kagramanov, and O. M. Nefedov, J. Am. Chem. Soc. **108**, 4352 (1986).

[9] F. A. Houle and J. L. Beauchamp, J. Am. Chem. Soc. **100**, 3290 (1978).

[10] J. W. Huang and W. R. M. Graham, J. Chem. Phys. **93**, 1583 (1990).

[11] G. Maier, H. P. Reisenauer, B. Rohde, and K. Dehnicke, Chem. Ber. **116**, 732 (1983).

[12] J. D. Getty, M. J. Burmeister, S. G. Westre, and P. B. Kelly, J. Am. Chem. Soc. **113**, 801 (1991).

[13] J. D. Getty and P. B. Kelly, Chem. Phys. **168**, 357 (1992).

[14] X. Liu, J. D. Getty, and P.B. Kelly, J. Chem. Phys. **99**, 1522 (1993).

[15] J. D. Getty, X. Liu, and P. B. Kelly, J. Phys. Chem. **96**, 10155 (1992).

[16] J. D. Getty, X. Liu, and P. B. Kelly, Chem. Phys. Letts. **201**, 236 (1993).

[17] E. Hirota, C. Yamada, and M. Okunishi, J. Chem. Phys. **97**, 2963 (1992).

[18] C. L. Currie and D. A. Ramsay, J. Chem. Phys. **45**, 488 (1966).

[19] A. B. Callear and H. K. Lee, Trans. Chem. Soc. **64**, 308 (1968).

[20] H. E. van der Bergh and A. B. Callear, Trans. Faraday Soc. **66**, 2681 (1970).

[21] N. Nakashima and K. Yoshihara, Laser Chem. **7**, 177 (1987).

[22] J. W. Hudgens and C. S. Dulcey, J. Phys. Chem. **89**, 1505 (1985).

[23] A. D. Sappey and J. C. Weisshaar, J. Phys. Chem. **91**, 3731 (1987).

[24] D. W. Minsek, J. A. Blush, and P. Chen, J. Phys. Chem. **96**, 2025 (1992).

[25] J. A. Blush, D. W. Minsek, and P. Chen, J. Phys. Chem. **96**, 10150 (1992).

[26] D. W. Minsek and P. Chen, J. Phys. Chem. **97**, 13375 (1993).

[27] D. W. Kohn, H. Clauberg, and P. Chen, Rev. Sci. Instrum. **63**, 4003 (1992); H. Clauberg, D. W. Minsek, and P. Chen, J. Am. Chem. Soc. **114**, 99 (1992); H. Clauberg and P. Chen, *ibid.* **113**, 1445 (1991).

[28] S. D. Peyerimhoff and R. J. Buenker, J. Chem. Phys. **51**, 2528 (1969).

[29] T. Takada and M. Dupuis, J. Am. Chem. Soc. **105**, 1713 (1983).

[30] C. Cometta-Morini, T. -K. Ha, and J. F. M. Oth, J. Molec. Struct. (Theochem) **188**, 79 (1989).

[31] E. Fjogstad and M. Ystenes, Spectrochim. Acta **46A**, 47 (1990).

[32] P. G. Szalay, A. G. Csaszar, G. Fogarasi, A. Karpfen, and H. Lischka, J. Chem. Phys. **93**, 1246 (1990).

[33] F. Sim, D. R. Salahub, S. Chin, and M. Dupuis, J. Chem. Phys. **95**, 4317 (1991).

[34] E. Hirota, J. Molec. Struct. **320**, 75 (1994).

[35] T. -K. Ha, H. Baumann, and J. F. M. Oth, J. Chem. Phys. **85**, 1438 (1986).

[36] J. M. Oliva, J. Gerratt, D. L. Cooper, P. B. Karadakov, and M. Raimondi, J. Chem. Phys. **106**, 3663 (1997).

[37] L. Farnell and W. G. Richards, J. C. S. Chem. Comm. 334 (1973).

[38] P. Merlet, S. D. Peyerimhoff, R. J. Buenker, and S. Shih, J. Am. Chem. Soc. **96**, 959 (1974).

[39] S. Olivella, A. Solé, and J. M. Bofill, J. Am. Chem. Soc. **112**, 2160 (1990).

[40] R. B. Woodward, R. Hoffmann, "The Conservation of Orbital Symmetry", Academic Press, 1970.

[41] H. C. Longuet-Higgins and E. W. Abrahamson, J. Am. Chem. Soc. **87**, 2045 (1965).

[42] G. Greig and J. C. J. Thynne, Trans. Faraday Soc. **62**, 3338 (1966).

[43] H. -J. Deyerl, T. Gilbert, I. Fischer, and P. Chen, J. Chem. Phys. **107**, 3329 (1997).

[44] A. M. Wodtke and Y. T. Lee, J. Chem. Phys. **89**, 4744 (1985).

[45] A. M. Wodtke (unpublished).

[46] D. Proch and T Trickl, Rev. Sci. Instrum. **60**, 713 (1989).

[47] D. Stranges, X. Yang, J. D. Chesko, and A. G. Suits, J. Chem. Phys. **102**, 6067 (1995).

[48] R. E. Continetti, B. A. Balko, and Y. T. Lee, J. Chem. Phys. **93**, 5719 (1990); R. E. Continetti, B. A. Balko, and Y. T. Lee, Chem. Phys. Letts. **182**, 400 (1991); B. A. Balko,

J. Zhang, and Y. T. Lee, J. Chem. Phys. **94**, 7958 (1991); D. A. Blank, S. W. North, and Y. T. Lee, Chem. Phys. **187**, 35 (1994).

[49] Y. T. Lee, J. D. McDonald, P. R. LeBreton, and D. R. Herschbach, Rev. Sci. Instrum. **40**, 1402 (1968).

[50] D. Stranges, A. G. Suits, and Y. T. Lee (to be published); D. A. Blank, S. W. North, D. Stranges, A. G. Suits, Y. T. Lee, J. Chem. Phys., **106**, 539 (1997).

[51] H. Okabe, "Photochemistry of small molecules", John Wiley & Sons, (1978).

[52] A. M. Schmoltner, Ph. D. Thesys, University of California, Berkeley (1989).

[53] W. L. Fitch and A. D. Sauter, Anal. Chem. **55**, 832 (1983).

[54] J. G. Frey and P. Felder, Mol. Phys. **75**, 1419 (1992).

[55] G. E. Busch and K. R. Wilson, J. Chem. Phys. **56**, 3638 (1972); R. N. Zare, Mol. Photochem. **4**, 1 (1972).

[56] K. Holtzhauer, C. Cometta-Morini, and J. F. M. Oth, J. Phys. Org. Chem. **3**, 219 (1990).

[57] M. J. Pearson and B. S. Rabinovitch, J. Chem. Phys. **42**, 1624 (1965).

[58] T. Ibuki, T. Murata, and Y. Takezaki, J. Phys. Chem. **78**, 2543 (1974).

[59] J. Niedzielski, J. Gawlowski, and T. Gierczak, J. Photochem. **21**, 195 (1983); M. Naroznik and J. Niedzielski, *ibid.* **32**, 281 (1986).

[60] J. I. Steinfeld, J. S. Francisco, and W. L. Hase, "Chemical kinetics and dynamics", Prentice-Hall, Englewood Cliffs, New Jersey (1989).

[61] CRC *Handbook of Chemistry and Physics*, edited by D. R. Lide (CRC Press, Boca Raton, 1992).

[62] The RRKM type $P(E_T)$ calculated for the reactions (3), (9), (11), and (12) give the same $<E_T>$ value.

[63] M. Yamaguchi, J. Molec. Struct. (Theochem.) **365**, 143 (1996).

[64] J. A. G. Dominguez and A. F. Trotman-Dickenson, J. Chem. Soc. 940 (1962).

[65] B. A. Balko, J. Zhang, and Y. T. Lee, J. Chem. Phys. **97**, 935 (1992); E. F. Cromwell, A. Stolow, M. J. J. Vrakking, and Y. T. Lee, *ibid.* **97**, 4029 (1992); A. Stolow, B. A. Balko, E. F. Cromwell, J. Zhang, and Y. T. Lee, J. Photochem. Photobiol. A: Chem. **62**, 285 (1992).

[66] Von B. Ondruschka, U. Ziegler, and G. Zimmermann, Z. Phys. Chemie, Leipzig **267**, 1127 (1986).

Table 1: RRKM microcanonical rate constants, A-factors, excitation energies E, and zero-point energy differences E_0 between transition state and reactant[a] for the reactions reported in Fig. 14.

Reaction	248 nm		351 nm			
	$k(E)/10^{10}$ (s^{-1})	E (kcal/mol)	$k(E)/10^{9}$ (s^{-1})	E (kcal/mol)	E_0 (kcal/mol)	logA
k_1	4.4	115.3	0.38	81.5	59.0[b]	13.7
k_2	2.6	115.3	0.03	81.5	68.1[c]	13.9
k_3	13.0	115.3	5.29	81.5	48.6[d]	13.6
k_{-3}	32.6	103.2	17.4	69.7	36.8[d]	13.1
k_4	3.9	115.3	1.62	81.5	49.8[e]	13.4
k_{-4}	11.6	100.0	7.44	66.2	34.5[e]	13.0
k_5	7.8	103.2	0.95	69.7	47.2[b]	13.2
k_6	19.1	100.0	7.46	66.2	40.5[f]	14.0
k_7	18.3	103.2	2.70	69.7	45.8[b]	13.4
k_8	19.5	100.0	2.92	66.2	43.2[b]	13.4
k_9	1.6	115.3	0.76	81.5	50.0[g]	13.3
k_{-9}	70.3	87.2	115	53.4	21.9[g]	13.3
k_{10}	1.1	87.2	0.00	53.4	52.9[h]	13.7

[a] ΔH_0 for reactants taken from Ref.'s 59 and 61.

[b] From Ref. 59 and references cited therein.

[c] A barrier of 20 kcal/mol for the reverse reaction is assumed (see text).

[d] From Ref. 66.

[e] From Ref. 58.

[f] From Ref. 64

[g] From Ref. 39.

[h] A barrier of 3 kcal/mol for the reverse reaction is assumed.

Table 2: Branching fractions for the different dissociation channels calculated with the Laplace transform method.[60]

Reaction products	Branching fraction at 248 nm	Branching fraction at 351 nm
$CH_2CCH_2 + H$	39.1% 28.1% from CH_2CHCH_2 11.0% from $CH_2C\bullet CH_3$	27.3% 16.8% from CH_2CHCH_2 10.5% from $CH_2C\bullet CH_3$
$CHCCH_3 + H$	34.5% 9.4% from $\bullet CHCHCH_3$ 25.1% from $CH_2C\bullet CH_3$	41.6% 11.7% from $\bullet CHCHCH_3$ 29.9% from $CH_2C\bullet CH_3$
$C_2H_2 + CH_3$	26.4% 16.8% from CH_2CHCH_2 9.6% from $\bullet CHCHCH_3$	31.1% 1.2% from CH_2CHCH_2 29.9% from $\bullet CHCHCH_3$
$c\text{-}C3H_4 + H$	0.1%	0.0%

FIGURE CAPTIONS

Figure 1: Schematic view of the apparatus. Photolysis laser is perpendicular to the plane of the figure. PV, pulsed valve; DET, detector; **E**, direction of the electric vector of the laser. The polarization angle γ is defined with respect to the detector axis as shown, and the laboratory scattering angle Θ is the angle between the molecular beam and the detector axis.

Figure 2: Pyrolytic free radical pulsed molecular beam source. a) pulsed valve, b) allumina insulator block, c) allumina standoff, d) SiC tube, e) allumina screws, f) electrodes, g) water cooled copper block.

Figure 3: Mass spectra of the molecular beam of ~0.2% allyl iodide in He taken with the pyrolytic nozzle at (a) room temperature (heat off) and (b) 1400 K (heat on).

Figure 4: Schematic view of the modified apparatus for H-atom detection. The photolysis laser is directed perpendicular to the plane of the figure. PV, pulsed valve; DET, detector. The molecular beam direction is perpendicular to the detector axis (Θ=90°).

Figure 5: TOF spectra at a laboratory angle of 90° for m/e=1 (H^+) and m/e=2 (D^+) from photodissociation of HI and DI at 248 nm. The open circles represent experimental data. The solid line is the calculated TOF from the convolution on the instrumental response functions of the experimental apparatus (neutral flight length, 36.7 cm; ionizer width, 0.9 cm).

Figure 6: TOF spectra for m/e 38 ($C_3H_2^+$) from photodissociation of the allyl radical at 248 nm at the indicated laboratory angles. The open circles are experimental points and the solid line is the simulation using the $P(E_T)$ in Fig. 7.

Figure 7: The center-of-mass transaltional energy distribution used to fit the data in Fig. 6.

Figure 8: TOF spectra for m/e = 26 ($C_2H_2^+$) from photodissociation of allyl radical at 248 nm at the indicated laboratory angles. The open circles are experimental points, the dashed line is the contribution from the C_2H_2 + CH_3 channel, the dotted line is the contribution from the C_3H_4 + H channel, and the solid line is the total fit to the data.

Figure 9: Newton diagram for allyl radical photodissociation at 248 nm. The circles represent the thermodynamic limit for each photofragment.

Figure 10: The center-of-mass translational energy distribution used to fit the contribution of C_2H_2+CH_3 photodissociation channel in figures 8 and 11.

Figure 11: TOF spectrum for m/e 15 (CH_3^+) from photodissociation of the allyl radical at 248 nm excitation at Θ=30°. The open circles are experimental points and the solid line is the simulation using the $P(E_T)$ in Fig. 10.

Figure 12: TOF spectra for m/e 39 ($C_3H_3^+$) from photodissociation of the allyl radical at 351 nm at the indicated laboratory angles. The open circles are experimental points and the solid line is the simulation using the $P(E_T)$ in Fig. 13.

Figure 13: The center-of-mass translational energy distribution used to fit the data in Fig. 12.

Figure 14: Dissociation and isomerization reaction schemes. Also reported are the unimolecular rate constants calculated by RRKM theory (Tab. 1).

Figure 15: An energy level diagram for the 248 and 351 nm photodissociation of the allyl radical.

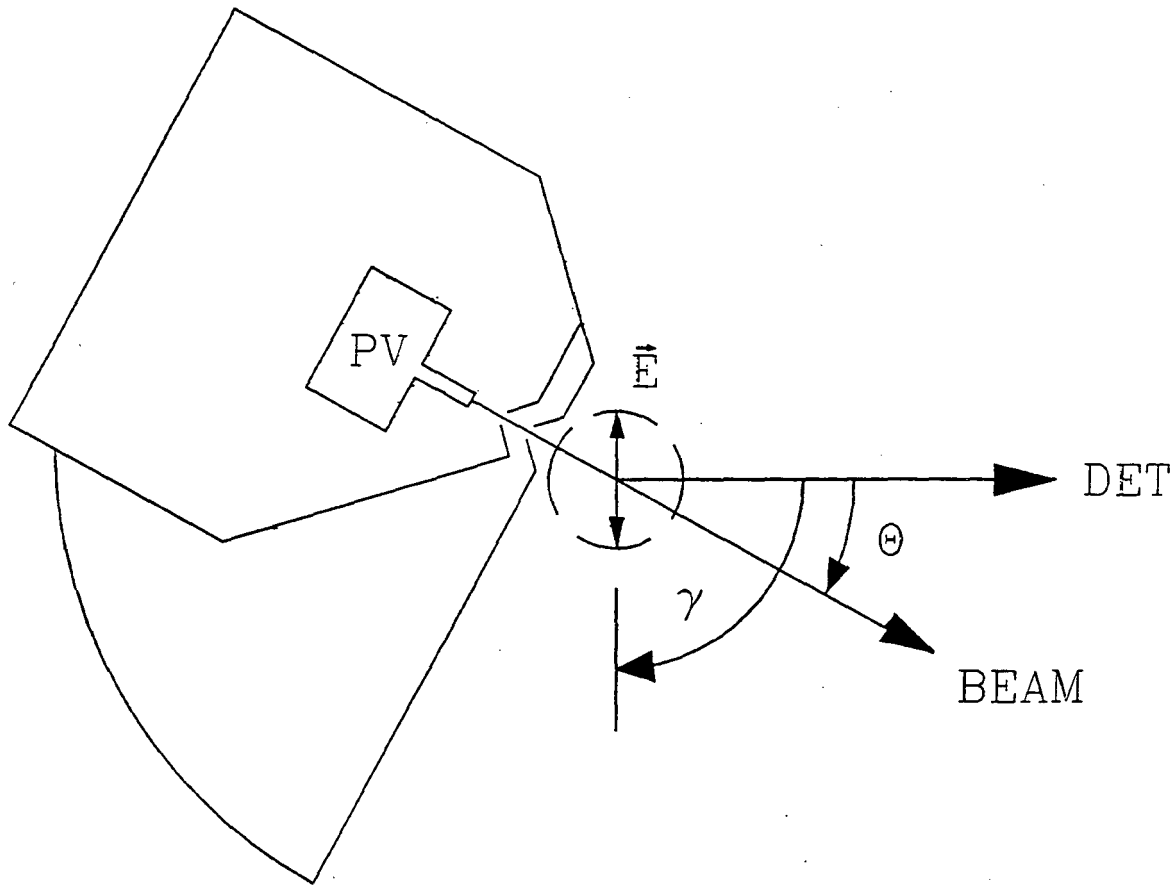

Figure 1

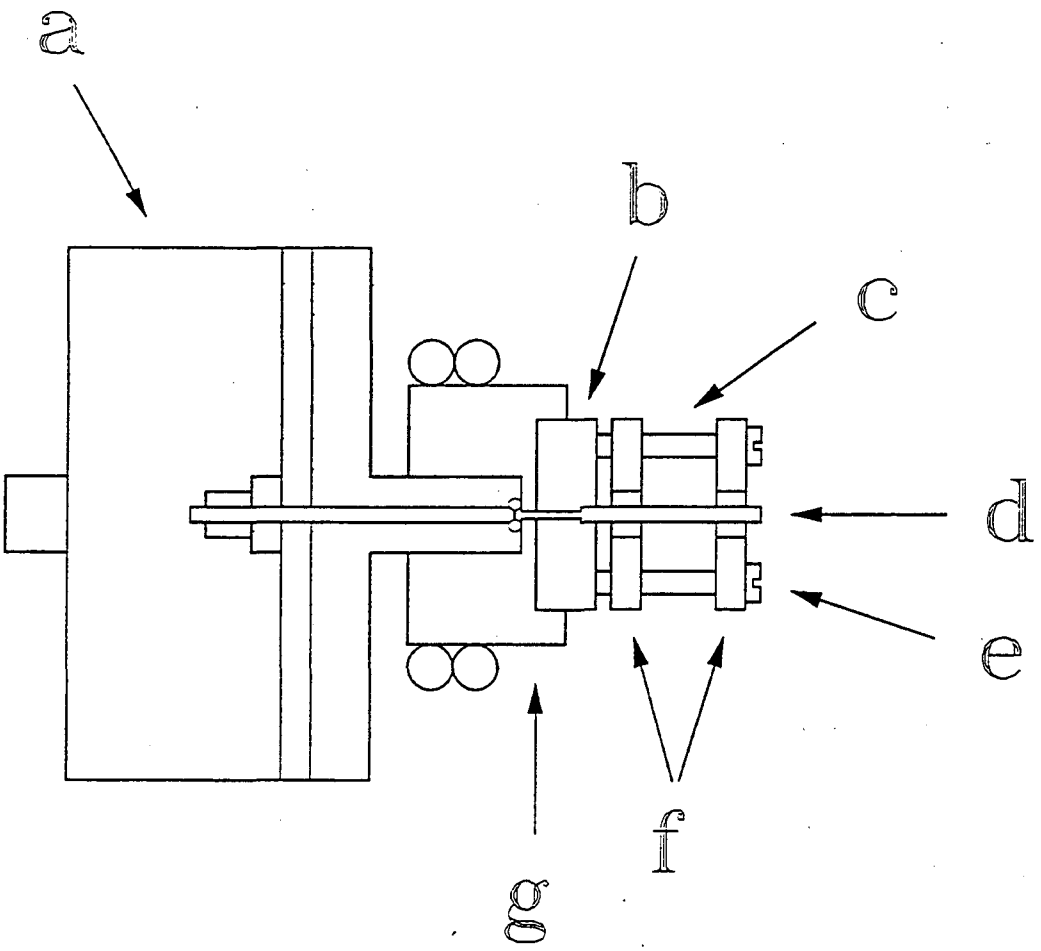

Figure 2

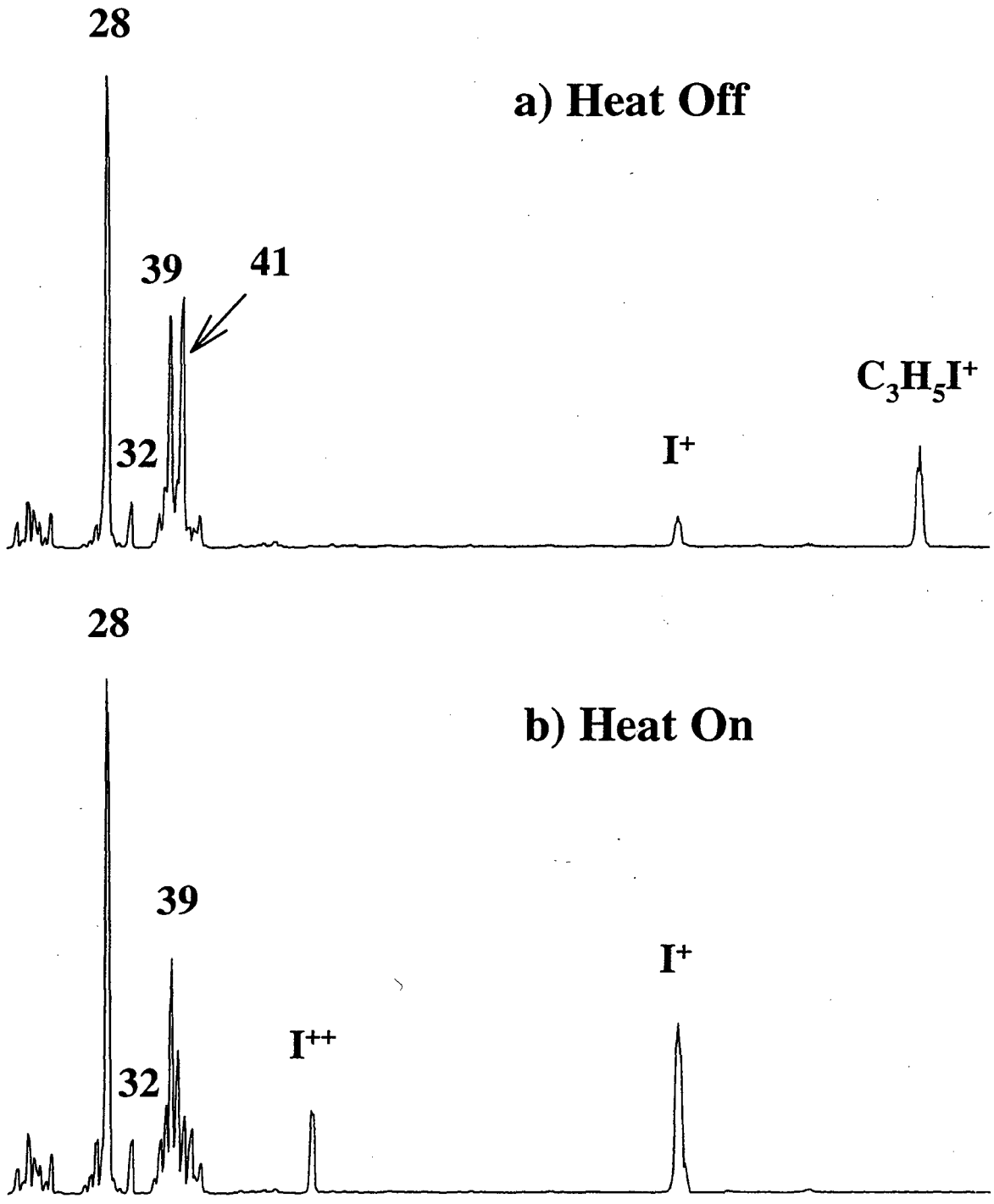

Figure 3

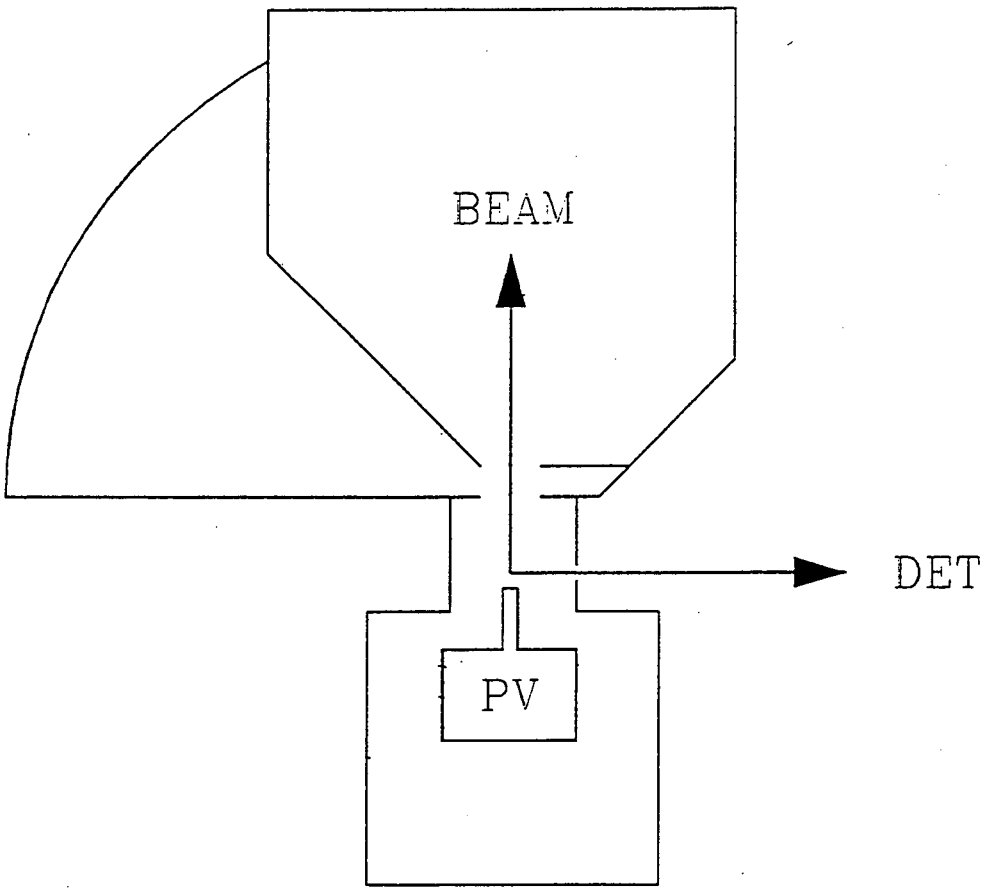

Figure 4

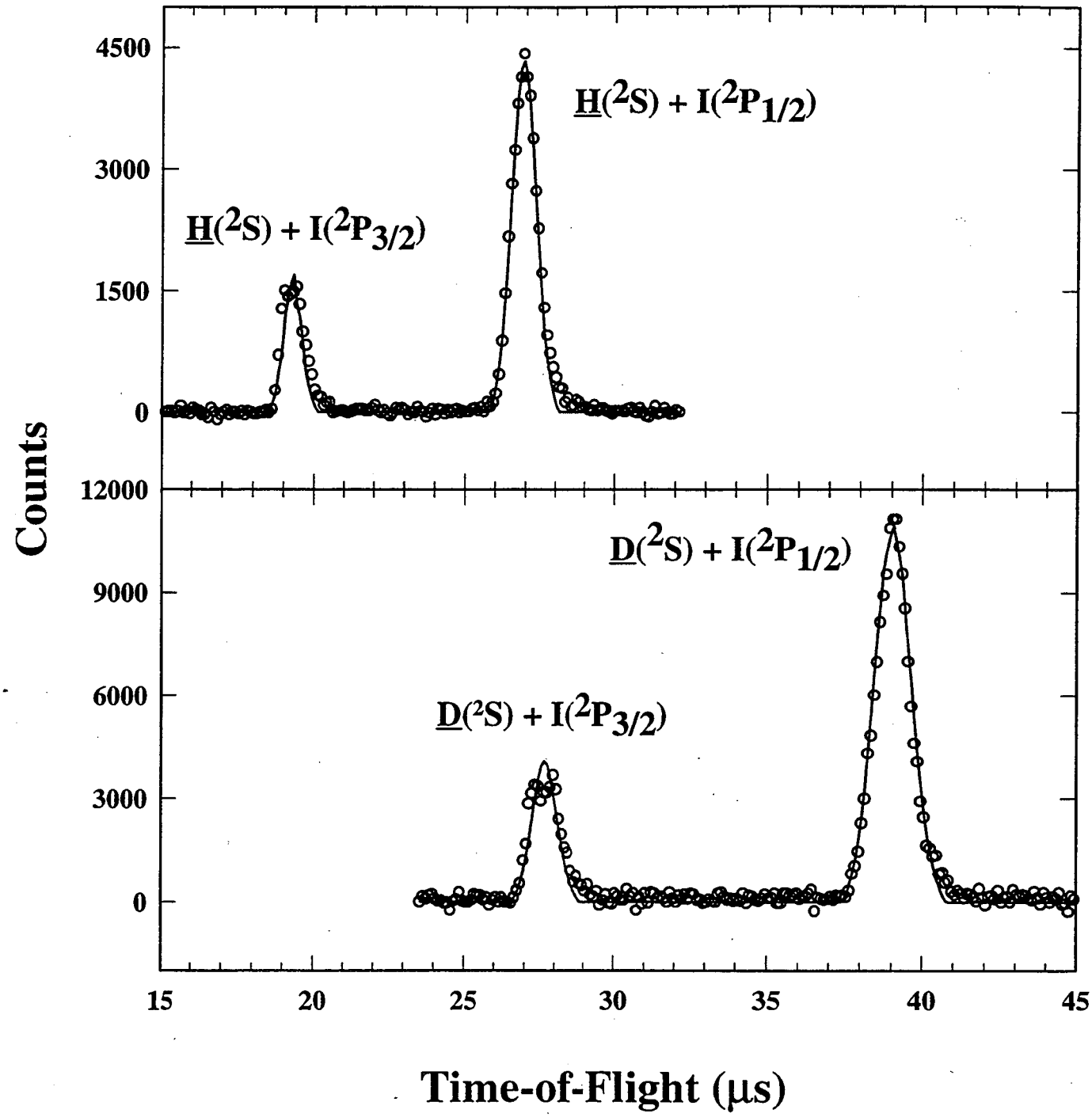
4500
3000
1500
0
H(2S) + I(2P3/2)
H(2S) + I(2P1/2)
12000
9000
6000
3000
0
D(2S) + I(2P3/2)
D(2S) + I(2P1/2)
Counts
15
20
25
30
35
40
45
Time-of-Flight (μs)

Figure 5

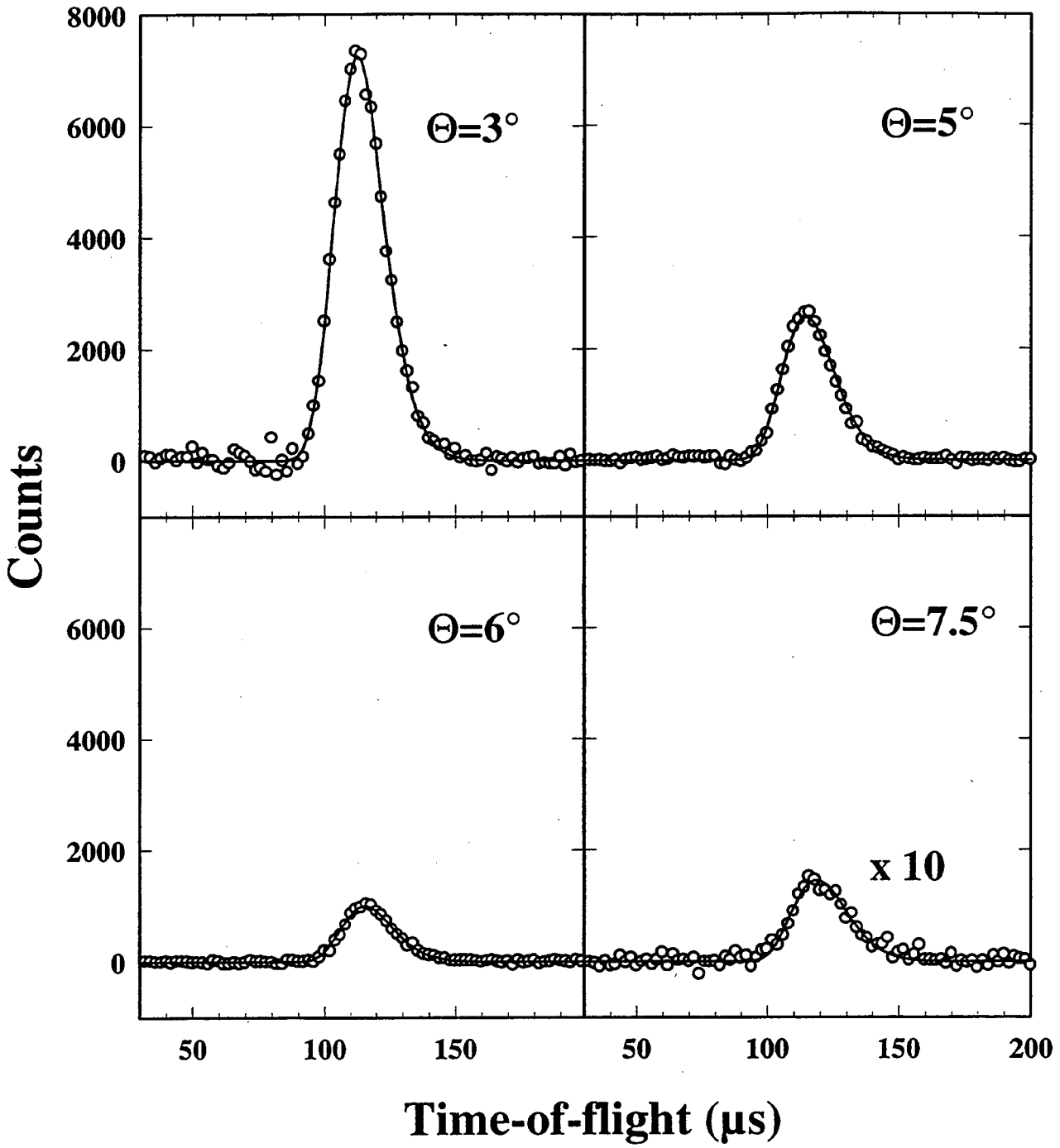
8000
6000
4000
2000
0
Counts
Θ=3°
Θ=5°
Θ=6°
Θ=7.5°
x 10
50
100
150
50
100
150
200
Time-of-flight (μs)

Figure 6

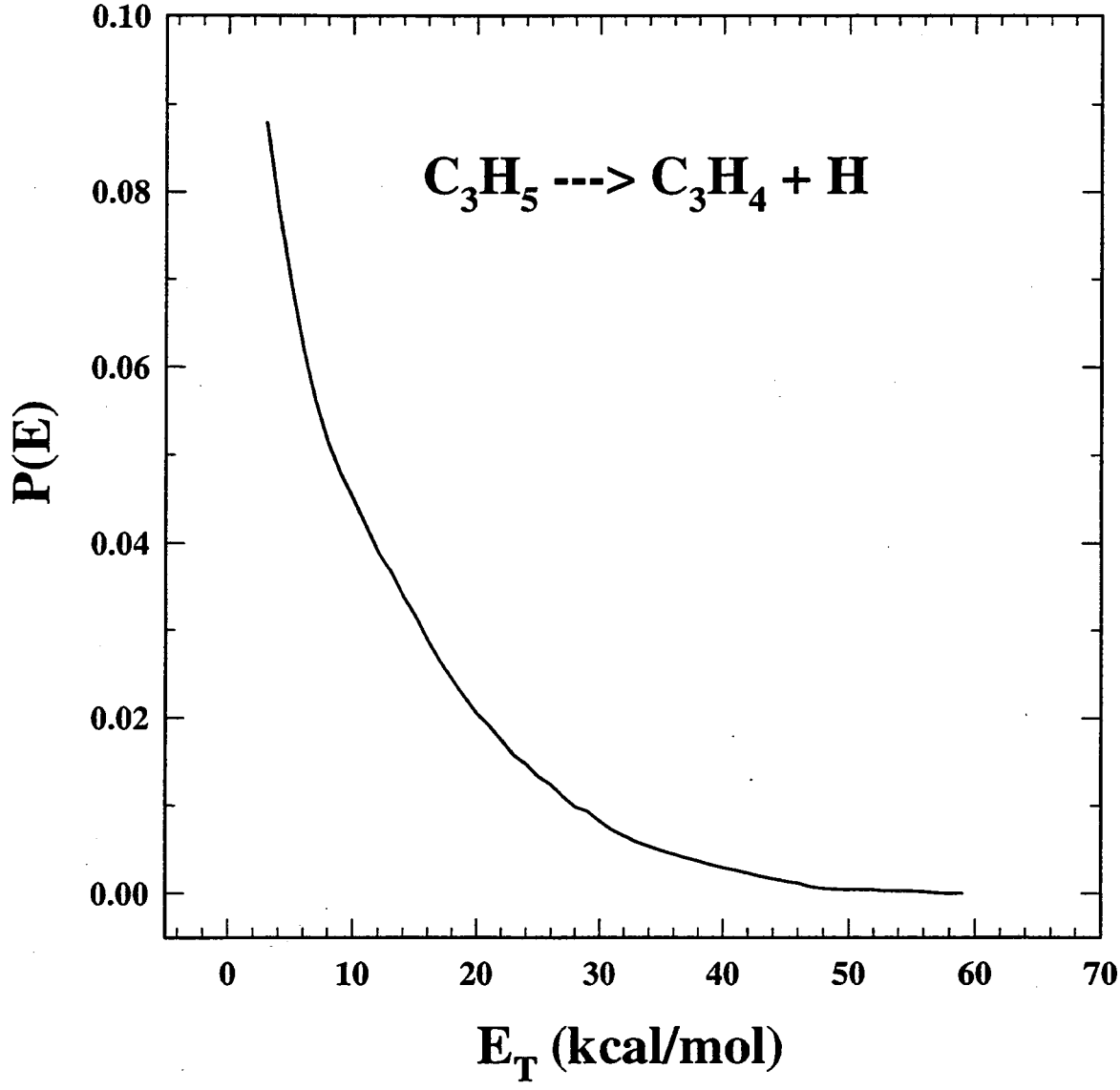
0.10
0.08
0.06
0.04
0.02
0.00
P(E)
C3H5 ---> C3H4 + H
0
10
20
30
40
50
60
70
ET (kcal/mol)

Figure 7

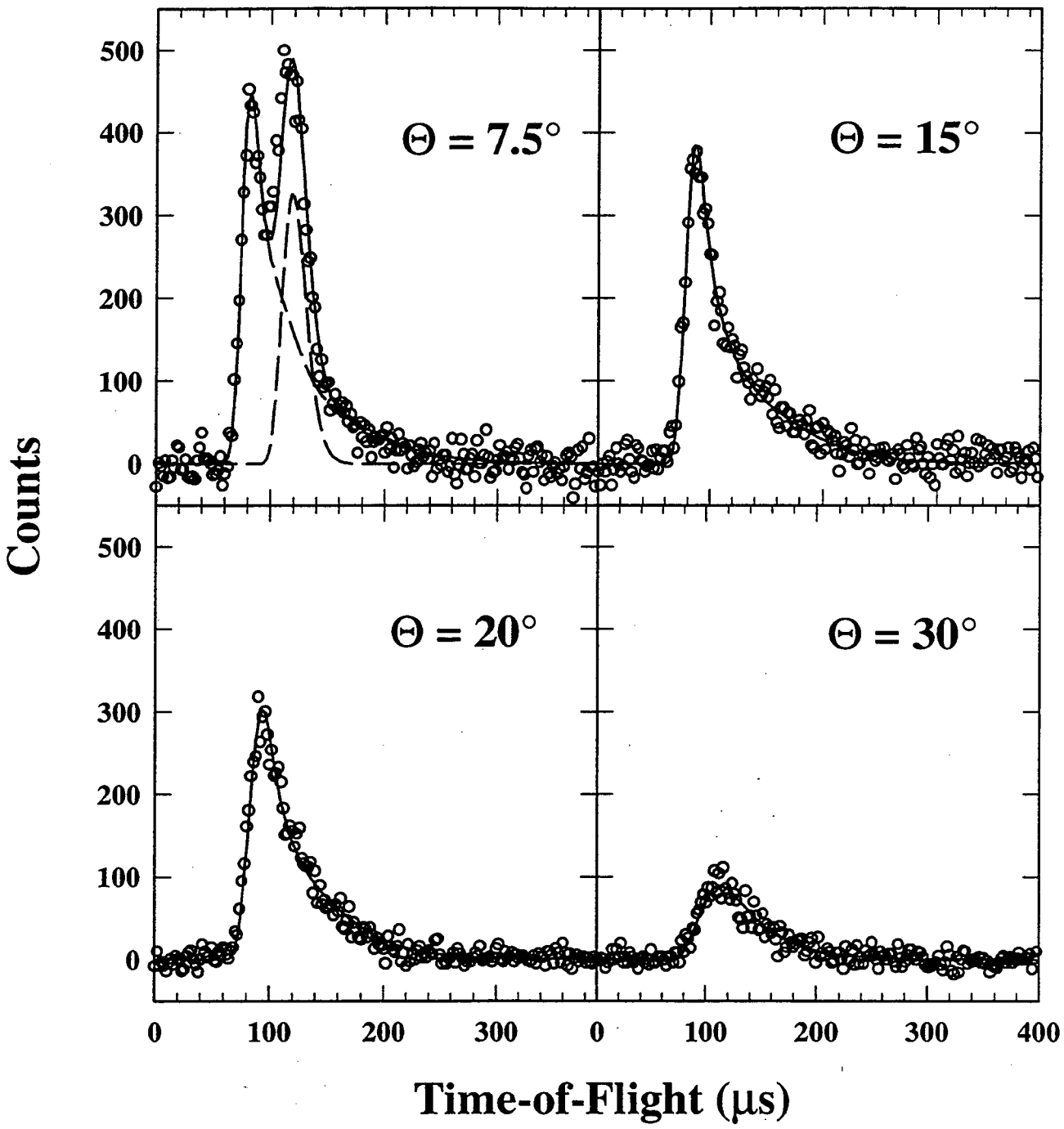

Figure 8

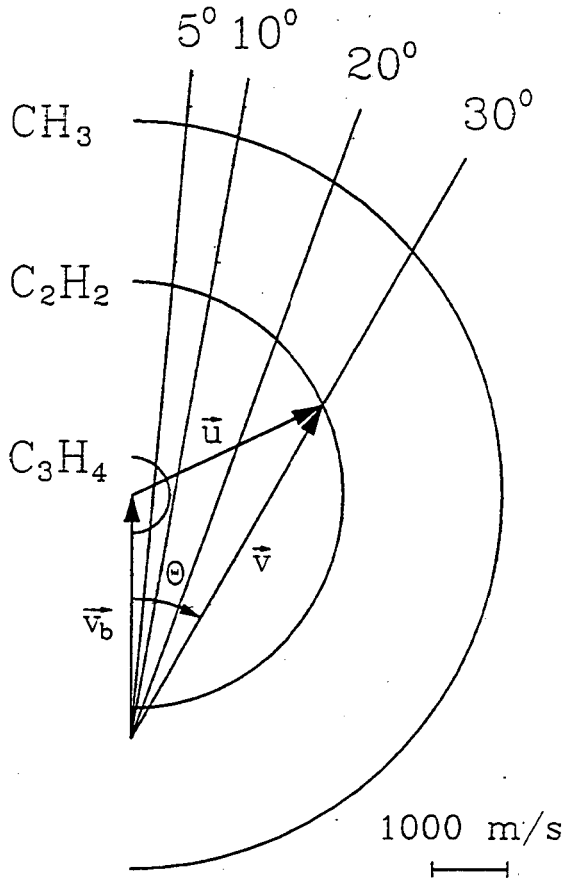

Figure 9

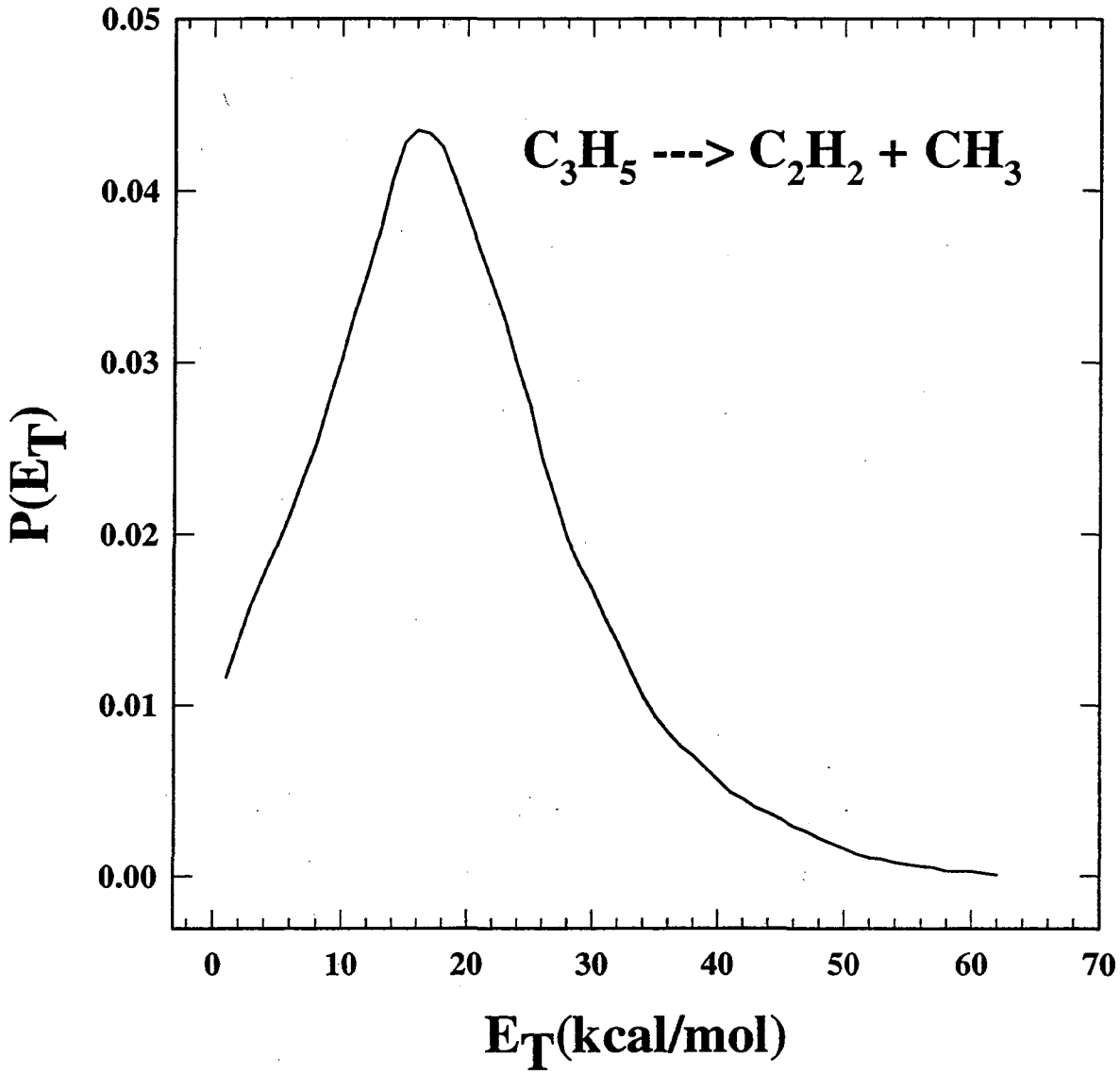
C_3H_5 ---> C_2H_2 + CH_3
P(E_T)
0.05
0.04
0.03
0.02
0.01
0.00
0
10
20
30
40
50
60
70
E_T(kcal/mol)

Figure 10

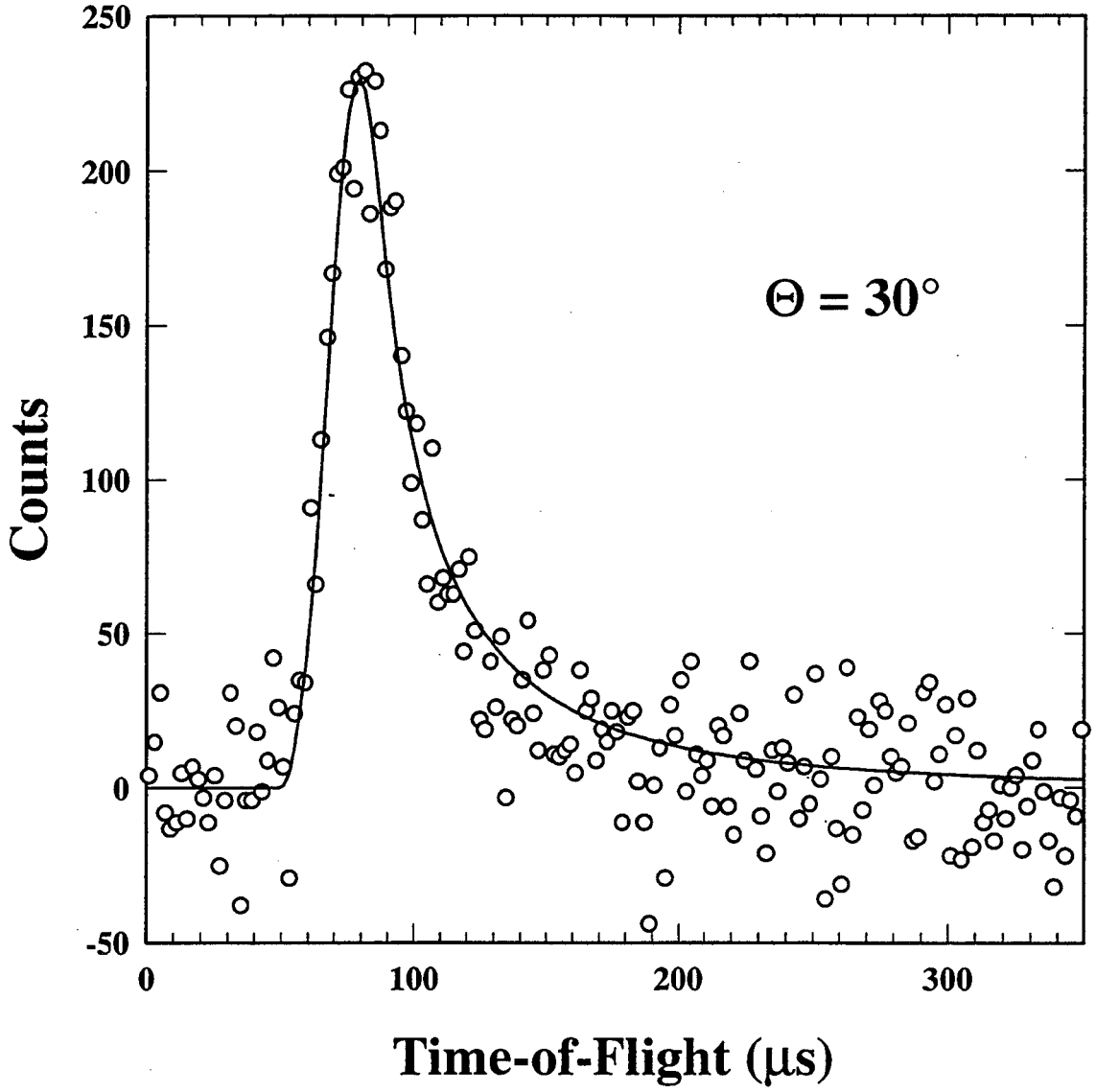
250
200
150
100
50
0
-50
0
100
200
300
Counts
Time-of-Flight (μs)
Θ = 30°

Figure 11

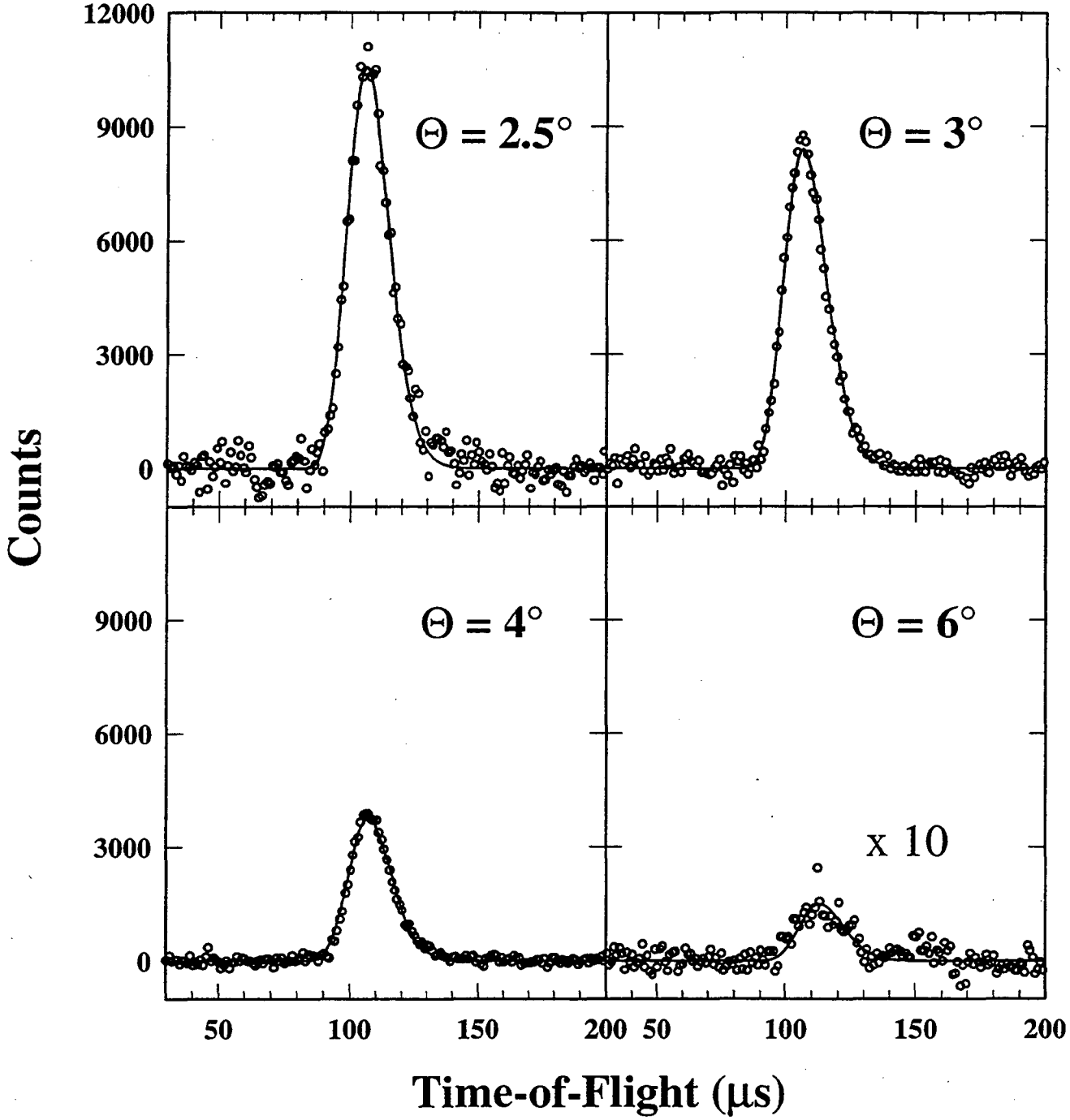
12000
9000
6000
3000
0
Θ = 2.5°
Θ = 3°
Θ = 4°
Θ = 6°
x 10
Counts
50
100
150
200
Time-of-Flight (μs)

Figure 12

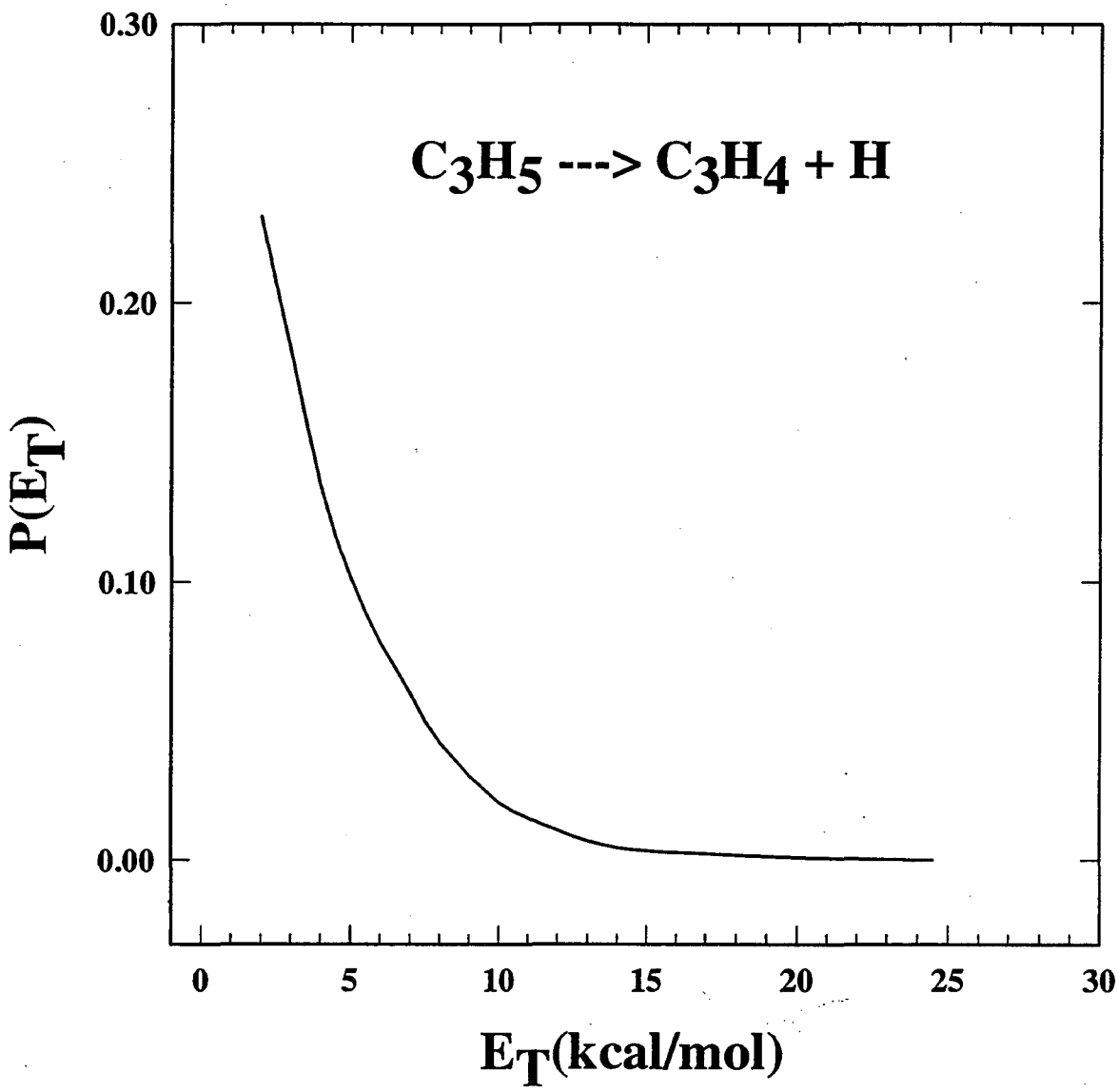

Figure 13

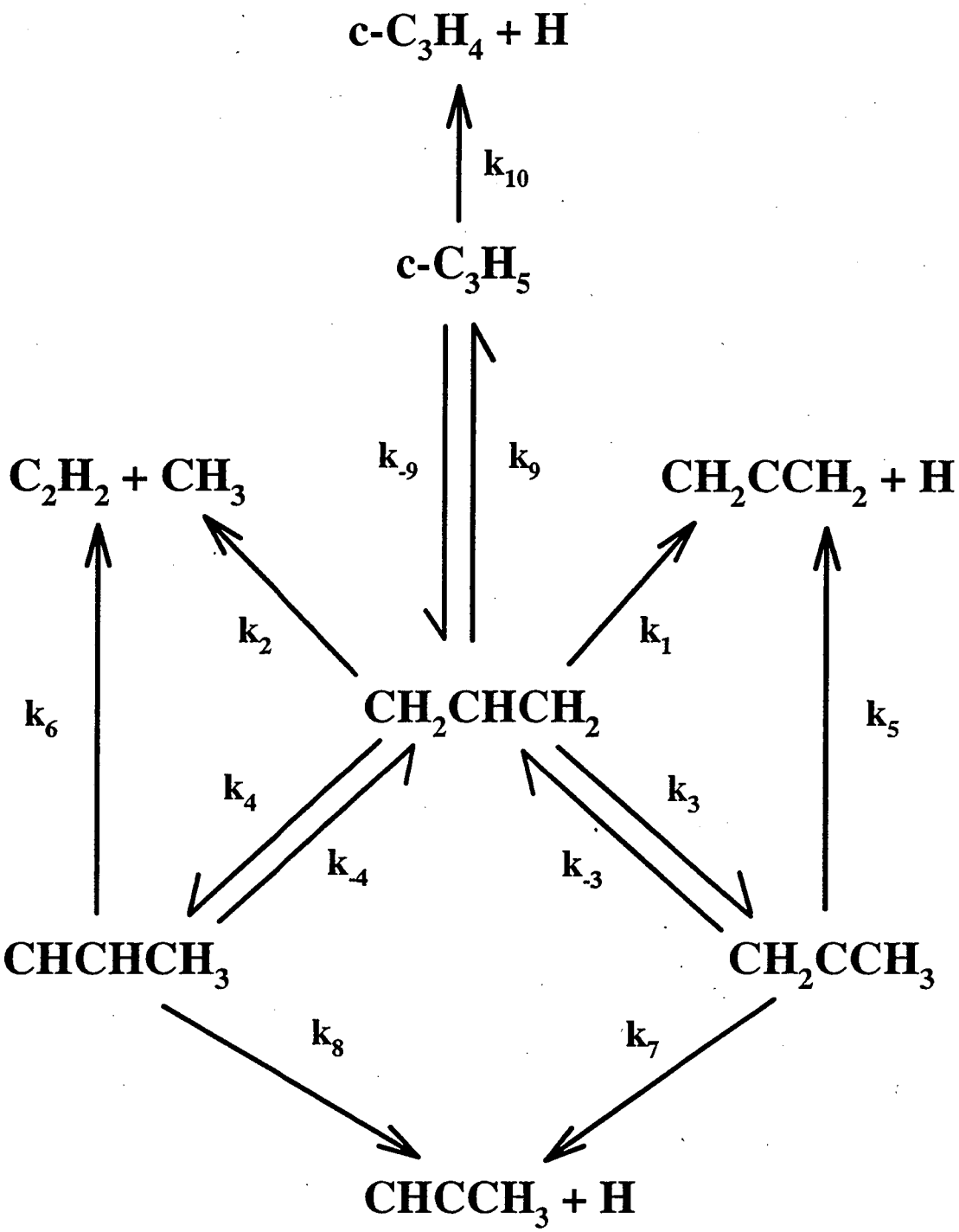
c-C3H4 + H
k10
c-C3H5
k-9
k9
C2H2 + CH3
CH2CCH2 + H
k2
k1
k6
CH2CHCH2
k5
k4
k3
k-4
k-3
CHCHCH3
CH2CCH3
k8
k7
CHCCH3 + H

Figure 14

Figure 15

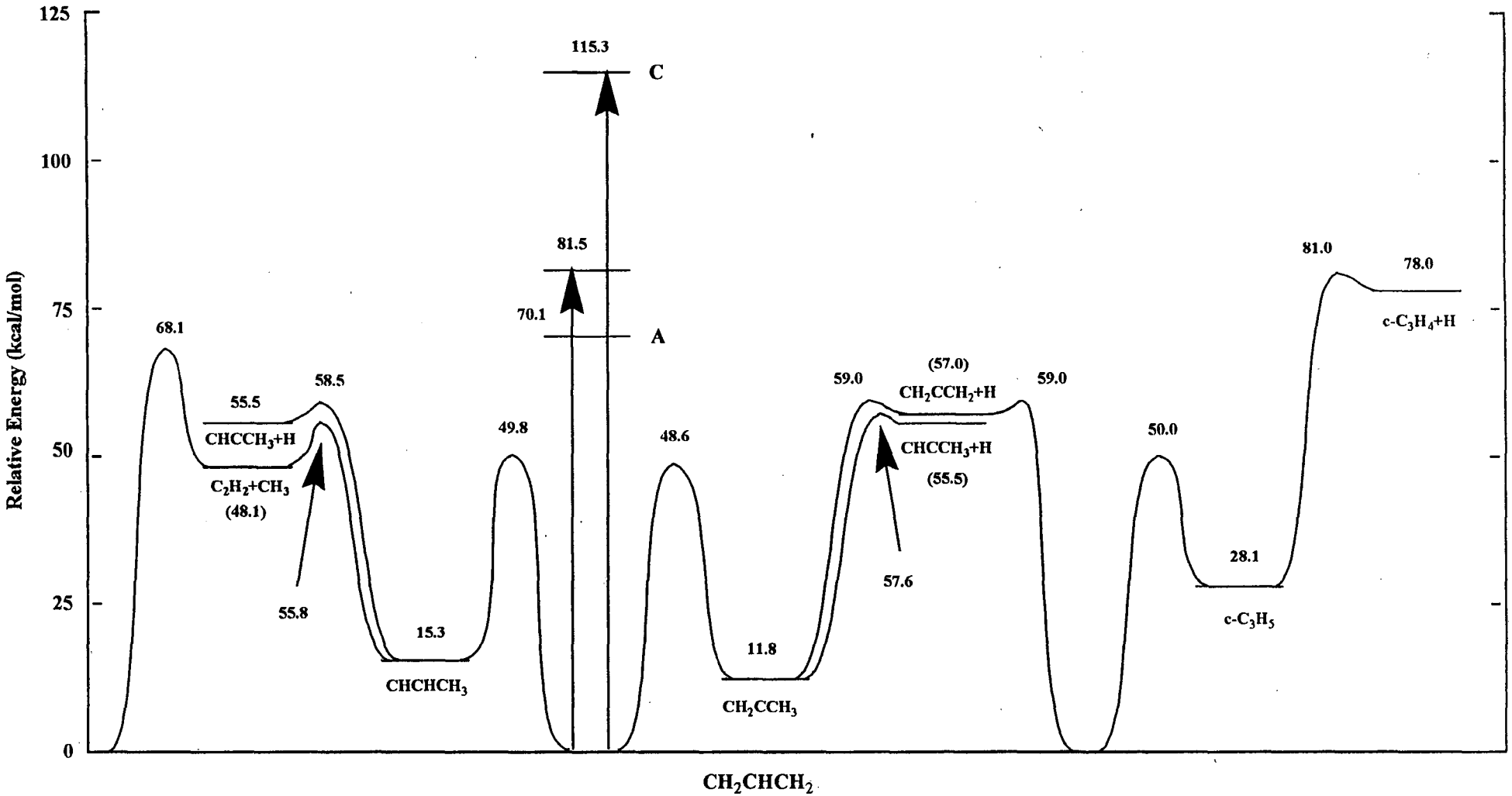
125
100
75
50
25
0
Relative Energy (kcal/mol)
115.3
C
81.5
70.1
A
68.1
55.5
CHCCH3+H
C2H2+CH3
(48.1)
58.5
55.8
15.3
CHCHCH3
49.8
48.6
11.8
CH2CCH3
59.0
(57.0)
CH2CCH2+H
CHCCH3+H
(55.5)
57.6
59.0
50.0
28.1
c-C3H5
81.0
78.0
c-C3H4+H
CH2CHCH2

Ernest Orlando Lawrence Berkeley National Laboratory
One Cyclotron Road | Berkeley, California 94720

Prepared for the U.S. Department of Energy under Contract No. DE-AC03-76SF00098